Capillary pressure as a unique function of electric permittivity and water saturation

Willem-Jan Plug,[1] Evert Slob,[1] Jan van Turnhout,[2] and Johannes Bruining[1]

Received 16 February 2007; revised 24 April 2007; accepted 5 June 2007; published 10 July 2007.

[1] The relation between capillary pressure (P_c) and interfacial area has been investigated by measuring P_c and the electric permittivity at 100 kHz simultaneously as function of the water saturation, (S_w). Drainage and imbibition experiments have been conducted for sand-distilled water-gas (CO_2/N_2) systems. The main capillary cycles and the scanning curves show hysteresis with the drainage curves displaying higher values than the imbibition curves. The 100 kHz permittivity data also show hysteresis between drainage and imbibition. Furthermore non-monotonic behavior is observed, which is analogous to the interfacial area characteristics obtained from network and micro-pore models. The permittivity behavior is attributed to polarization of the gas-water and water-solid interfaces. The permittivity hysteresis is provoked by the different phase distributions and geometries. Our results show that P_c is a unique function of the permittivity and S_w, and therefore this work provides clear evidence that the permittivity is a measure for the interfacial area. **Citation:** Plug, W.-J., E. Slob, J. van Turnhout, and J. Bruining (2007), Capillary pressure as a unique function of electric permittivity and water saturation, *Geophys. Res. Lett.*, *34*, L13306, doi:10.1029/2007GL029674.

1. Introduction

[2] Capillary pressure (P_c) plays an important role in geosciences, e.g., hydrocarbon recovery, vadose zone hydrology, carbon dioxide sequestration, and soil remediation techniques. However, one may also think on porous tissue applications of biology and bioengineering. One of the key issues concerning capillary pressure is the non-uniqueness between the drainage (decreasing water saturation) and imbibition (increasing water saturation) processes on a continuum scale, the so-called capillary hysteresis. This non-uniqueness makes it difficult to predict the distributions of multiple fluids in a porous medium and the state of the system. Therefore, capillary pressure hysteresis is important in production environments using alternating water/gas injection processes known as WAG (Water Alternating Gas). Also the movement of oil in a heterogeneous reservoir and the success of soil remediation will be characterized by a sequence of drainage and imbibition events. From thermodynamic considerations it can be shown that P_c is the surface free-energy change that occurs when a unit of non-wetting fluid phase is injected or produced [*Morrow*, 1970; *Hassanizadeh and Gray*, 1993]. This macro-scale P_c is defined as the exterior pressure difference between the two phases, which depends on the interior water saturation (S_w). To get a better understanding of the capillary pressure behavior, we have investigated the capillary pressure and its relation to both S_w and the complex permittivity, ε_s^*.

[3] It has been suggested that P_c can be defined uniquely by S_w and the interfacial area [*Reeves and Celia*, 1996; *Held and Celia*, 2001; *Cheng et al.*, 2004]. In general a distinction is made between the capillary dominated interface between the wetting and non-wetting phase, α_{wn}, and the interface between the wetting and solid phase, α_{ws} [*Cheng et al.*, 2004]. In principle α_{wn} can be measured with interfacial tracers [*Dalla et al.*, 2002] and with micro-models [*Cheng et al.*, 2004]. However, these experiments are complicated and time-consuming. Theoretical and computational approaches, e.g. pore-scale network models, are also used to estimate α_{wn} [*Reeves and Celia*, 1996; *Held and Celia*, 2001]. In general, the functional relation between P_c, α_{wn} and S_w follows a general trend, is smooth and has a convex non-monotonic shape [*Hassanizadeh and Gray*, 1993; *Held and Celia*, 2001].

[4] We propose that the electric permittivity provides new insight in the understanding of the fundamentals and physical behavior of capillary pressure as function of the interfacial area. Examples of permittivity behavior in porous media can be found in the work of *Knight and Nur* [1987], *Ruffet et al.* [1991], *Knight* [1991], *Knight and Abad* [1995], *Roberts and Lin* [1997], *Chelidze and Gueguen* [1999], *Chelidze et al.* [1999], *Seleznev et al.* [2004], and *Plug et al.* [2007]. All these authors reported on the permittivity response in the frequency range, from 1 to 14 MHz. In a previous paper [*Plug et al.*, 2007] we presented a novel set-up with which we can measure P_c and ε_s^* simultaneously as function of S_w for gas-water systems. We showed that a small hysteresis in the real part of the electric permittivity was observed for 3 MHz. As interfacial contributions of thin water layers play a minor role at such high frequencies we have attributed the hysteresis to a different distribution of the phases in the porous medium. It has been suggested in the literature that at lower frequencies, below 1 MHz, other mechanisms also contribute, such as ionic transport, polarization of the electrical double layer [*Chelidze et al.*, 1999; *Ulrich and Slater*, 2004] and conduction by surfactants adsorbed at the water-gas interface [*Knight*, 1991]. These mechanisms have in common that their contribution to the electric permittivity is caused by *interfacial* phenomena. Therefore, if it is possible to show experimentally that the capillary pressure is a unique function of water saturation and electric permittivity this

[1]Department of Geotechnology, Delft University of Technology, Delft, Netherlands.
[2]Faculty of Applied Sciences, Delft University of Technology, Delft, Netherlands.

0094-8276/07/2007GL029674$05.00

would support the idea that the capillary pressure is a unique function of water saturation and interfacial area.

[5] For this reason we present the experimental results from combined measurements of capillary pressure and the complex permittivity at 100 kHz as a function of S_w, using the set-up discussed by *Plug et al.* [2007]. The experiments were conducted for the sand-distilled water-gas (CO_2/N_2) systems at various fluid pressures (1-13 bar). We measured primary drainage and secondary imbibition curves and corresponding scanning curves for the intermediate water saturations.

2. Experimental Technique

[6] We used unconsolidated quartz sand samples with an average grain size fraction of $360 < D_{50} < 410$ micron. The sample holder consists of 3 parts: two stainless steel end-pieces and a non-conductive PEEK (Polyetheretherketone) ring. The untreated sample, with a diameter of 84 mm and a height of 27 mm, was placed in the sample holder and vibrated for 10 minutes. In order to support the sample, two types of metallic filters are used, which are placed inside the end-pieces.

[7] To measure the permittivity, a component analyzer (Wayne-Kerr, 6640A) is connected to the sample holder, whereby the two stainless steel end-pieces, the support filters included, act as electrodes. Our set-up contains two pressure transducers to monitor the water and gas pressure, a pressure difference transducer that records the capillary pressure and two syringe pumps, which can be set to a constant injection/production rate or to a constant pressure. A detailed description of the experimental set-up and sample holder is presented by *Plug et al.* [2007]. In the experiments we used distilled water as the wetting phase and N_2 or CO_2 as the non-wetting phase. We define P_c as the difference in bulk water and gas phase pressure, measured by the pressure difference transducer. The water saturation is determined from the produced or injected water volume. In this study different pressure conditions were investigated and the experiments were conducted at a constant temperature (temperature stability ≤ 0.5°C).

[8] To perform a capillary cycle, we initially saturated the evacuated sample with water. We started with a dewatering stage (primary drainage) and before the connate water saturation was reached the flow direction was changed and the secondary imbibition was conducted. Different drainage and imbibition scanning curves were obtained after the first cycle had been measured. Injection and production flow rates were less than 0.5 ml/hr in all cycles.

[9] During the displacement processes the impedance amplitude, $|Z|$ [Ω], and phase angle, θ [rad], were measured as a function of the frequency (f) and are related to the complex permittivity (ε_s^*) of the sample, defined by $\varepsilon_s^* = \varepsilon_s' - i\varepsilon''$. Here ε_s' and ε_s'' represent the real and the imaginary part of the permittivity respectively. We used air measurements [*Plug et al.*, 2007] to correct for additional impedance effects and parasite capacitances, caused by background noise, the sample holder configuration, the influence of the connecting cables and possible electrode polarization [*Chelidze et al.*, 1999; *Roberts and Lin*, 1997]. We calibrated the tool for materials with known permittivities in the range from 2 to 25 [−]. The measurements were compared with theoretical values and high precision and good agreement was found [*Plug et al.*, 2007].

3. Experimental Results

[10] Data for P_c and ε_s' were obtained on four different samples (S1-S4) for the N_2-water-sand and CO_2-water-sand systems in the fluid pressure range from atmospheric pressure to 13 bar and temperatures between 27 and 28°C. Figure 1 shows the $P_c - S_w$ curves for two N_2 experiments conducted at atmospheric pressures (S1) and 8 bar (S2a,b). In Figure 2 we show the capillary pressure curves for the drainage and imbibition cycles with CO_2 at pressures of 8 bar (S3a,b) and 13 bar (S4a-f). Different $P_c - P_w$ scans (S4c-f) at 13 bar CO_2 were conducted in the intermediate water saturation range of $0.41 < S_w < 0.78$. Comparison of the primary drainage and secondary imbibition $P_c - P_w$ curves for both the N_2 and CO_2 experiments show similar values for the drainage capillary pressure and agree within the experimental error, except at low water saturations. For both N_2 and CO_2 the drainage and imbibition capillary cycles show the conventional hysteresis for a water-wet porous medium, with the primary drainage curve showing higher values than the secondary imbibition curve. For the scanning curves measured at 13 bar (see Figure 2, S4c−S4f) the expected behavior was observed, because each curve lies between the primary drainage and secondary imbibition curve.

[11] In Figures 3 and 4 we show ε_s' as function of S_w for the N_2 and CO_2 experiments at $f = 100$ kHz and $f = 3$MHz, respectively. In the 3 MHz case (the dashed curves in Figures 3 and 4), ε_s' shows a small hysteresis and all the curves follow a monotonic behavior. Furthermore, the permittivity scanning curves (Figure 4, S4c−f) coincide with the secondary imbibition curve (S4b). At a frequency of 100 kHz and at $S_w < 1$, ε_s' clearly shows hysteresis between the primary drainage curves (S2a, S3a and S4a) and the corresponding secondary imbibition curves (S2b, S3b and S4b). In all cases ε_s' during secondary imbibition was higher than during primary drainage, except near the residual gas saturation. Here the imbibition curves decline steeply (see S2b in Figure 3 and S3b in Figure 4). The non-monotonic behavior in ε_s' (100 kHz), observed for the main capillary cycle, was reproduced in all experiments (see Figures 3 and 4). It shows a maximum at $S_w = S_{w,m}$, and has a smooth appearance. The 100 kHz measurements can attain values that are twice as high as for the high frequency case. However, at $S_w = 1$, the low frequency ε_s' coincides with the values measured at high frequency (3 MHz) for all experiments and it is most likely that the values would coincide in the same way for $S_w = 0$. It is clear that the small gas solubility does not affect the low frequency permittivity, because a similar behavior was obtained for both the almost insoluble N_2 and the slightly soluble CO_2.

[12] For the N_2 experiments as presented in Figure 3, ε_s' during primary drainage at 8 bar (S2b) was higher than ε_s' measured for atmospheric conditions (S1). We were not able to check the reproducibility of this result. However, the behavior for both pressure conditions was similar and for both cases the maximum value of ε_s' was found at $S_{w,m} \approx 0.85$. During secondary imbibition (S2b), $S_{w,m}$ decreased towards 0.72. From Figure 4, it is clear that the difference in

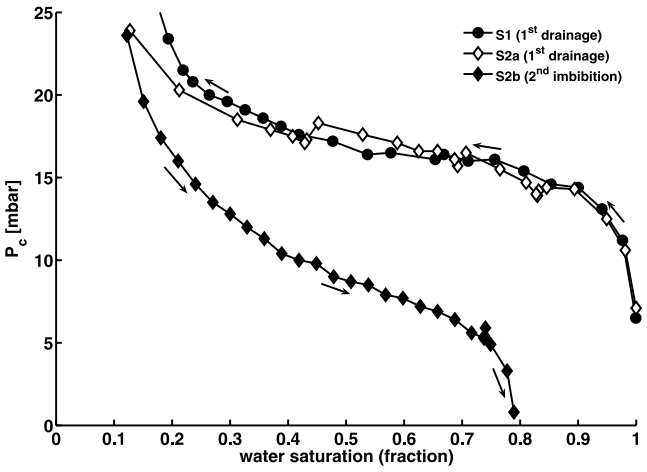

Figure 1. Capillary pressure curves for the N_2-sand-water system at atmospheric pressure (S1) and 8 bar (S2a, b). Hysteresis between the primary drainage (S2a) and the secondary imbibition (S2b) for the 8 bar N_2 experiment is clearly visible.

$S_{w,m}$ between the primary drainage and the secondary imbibition process for the CO_2 experiments was much smaller. In both cases $S_{w,m} \approx 0.8$ and $S_{w,m}$ for drainage was only slightly higher than for imbibition. Remarkable is that the primary drainage curves at 100 kHz for the CO_2 experiments coincide, whereas the secondary imbibition curve measured at 8 bar (S3b) lies above the 13 bar imbibition curve (S4b).

[13] Surprisingly, the permittivity scanning curves at 100 kHz as presented in Figure 4, show that the drainage curves (S4c and S4e) lie above the imbibition curves (S4d and S4f). This is contrary to the main capillary cycle, where ε'_s is higher for secondary imbibition than for primary drainage. Moreover, the permittivity scanning curves approximate the secondary imbibition curve (S4b), where the drainage curves (S4c and S4e) are higher and the imbibition curves (S4d and S4f) are lower than the secondary imbibition curve.

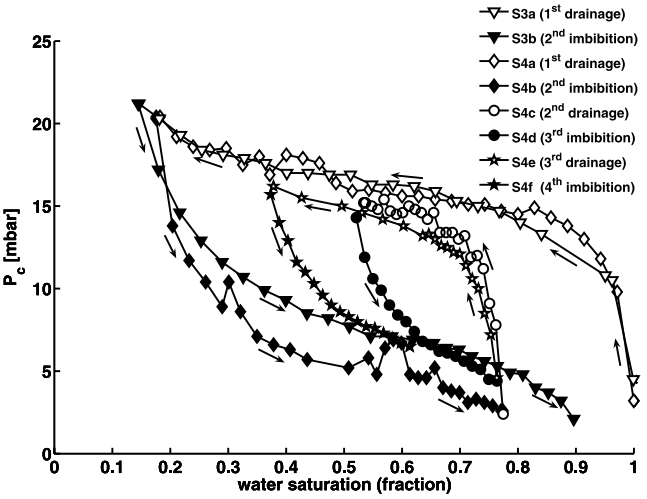

Figure 2. Capillary pressure curves for the CO_2-sand-water system at 8 bar (S3a, b) and 13 bar (S4a-f). The primary drainage curves (S3a and S4a) for both pressure conditions coincide. For the secondary imbibition (S3b and S4b) a shift in capillary pressure is observed. The capillary pressure hysteresis for water-wet porous media is observed, where the drainage curves lie above the imbibition curves. For the 13 bar CO_2 experiment, drainage (S4c, S4e) and imbibition (S4d, S4f) scans are measured and are in between the primary drainage and secondary imbibition curve.

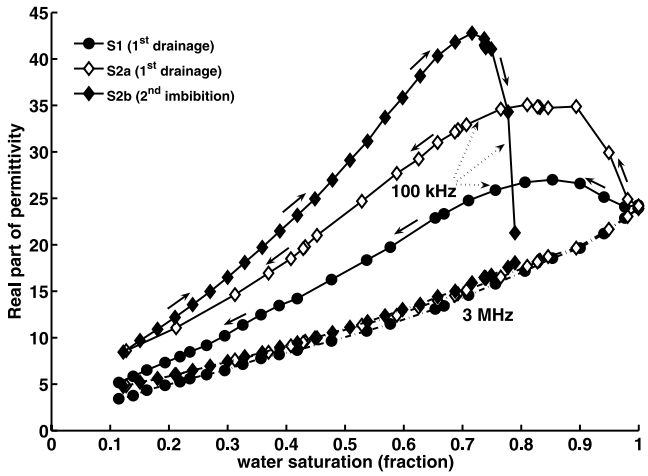

Figure 3. ε'_s (real part of the complex permittivity ε^*_s) as function of S_w for the N_2-sand-water system. S1 and S2a represent the primary drainage curves for the atmospheric and 8 bar pressure conditions, respectively. S2b is the secondary imbibition curve for the 8 bar case. The solid lines represent ε'_s for the 100 kHz and the dashed lines the 3 MHz. The permittivity for the 3 MHz shows small hysteresis between the drainage (S2a) and the imbibition (S2b). The permittivities obtained for 100 kHz show non-monotonic behavior and hysteresis where the imbibition curve (S2b) lies above the drainage curve (S2a).

4. Discussion

[14] The high frequency permittivity data (3 MHz) followed the typical behavior of one of the mixing rules and are monotonic [see *Plug et al.*, 2007]. Hence, for increasing water saturations, the electric permittivity increases steadily. However, the 100 kHz data (Figures 3 and 4) show no steady rise for increasing S_w, but a non-monotonic behavior of ε'_s as function of the water saturation. We attribute this behavior to polarization effects, occurring at the solid-water and the water-gas interfaces of water layers. Additionally, ionic transport in the water layers will cause the build-up of double layers and contributes to the permittivity measured at 100 kHz.

[15] The trajectory of the low frequency permittivity as function of the water saturation is interpreted using percolation theory and strongly depends on the presence of the gas phase. During (primary) drainage the gas phase, will first penetrate the larger pores, resulting in an increase in electric permittivity. This is the case during the first stage of the primary drainage curves, where already for small amounts of gas, ε'_s increases rapidly to a maximum. This may be explained by increasing water-gas interfaces. The sand sample is completely water-wet ($P_c > 0$) meaning that

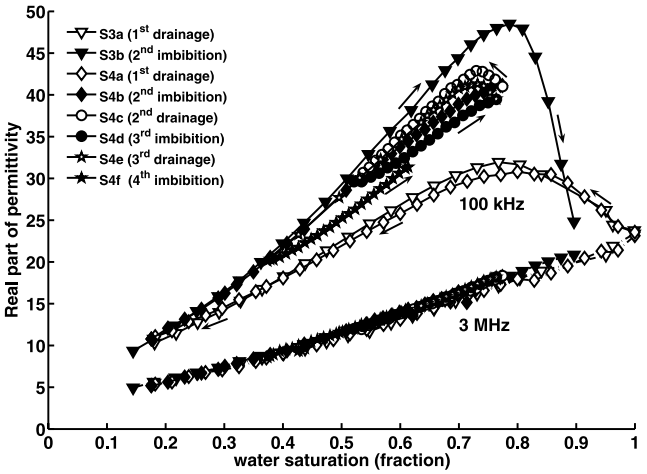

Figure 4. The permittivity as function of S_w for the CO_2-sand-water system. S3a and S4a represent the primary drainage curves for the 8 bar and 13 bar pressure conditions, respectively and S3b and S4b are the secondary imbibition curves. The solid lines represent ε'_s for the 100 kHz case and the dashed lines the 3 MHz case. The low frequency curves clearly demonstrate hysteresis and non-monotonic behavior is observed where the secondary imbibition curves (S3b and S4b) are above the primary drainage curves (S3a and S4a). The 3 MHz, scanning curves (S4c-f), conducted for the 13 bar CO_2 case, coincide with the secondary imbibition curve. At 100 kHz, the drainage scanning curves (S4c, e) lie above the imbibition curves (S4d, f) and approximate the secondary imbibition curve.

all the grains are coated with a thin water layer. These water layers can become extremely thin on the convex side of the grains for which the nearby pores are filled with gas that protrudes the water-filled pores. Percolation theory suggests that the capillary pressure must be high enough for the gas to invade these pores. This is the case when the number of allowed pores, which are big enough for the gas to invade, exceeds the percolation threshold. This percolation threshold, where the gas phase forms a continuous path, is reached at the point where ε'_s shows a maximum at $S_w = S_{w,m}$. As the gas pressure increases further, and thus the capillary pressure still increases, the electric permittivity decreases. We understand this as gas saturation increases, and a large part of the water in the thin layers is "bound' to the grains (not free), rotation of the dipole orientations of the water molecules in these thin films becomes difficult under the presence of an electric field. This results in relatively weak polarization effects. The hysteresis in electric permittivity as observed between the primary drainage (e.g., S4a in Figure 4) and secondary imbibition process (e.g., S4b in Figure 4) can be explained by different phase geometries and surface water distributions (clusters).

[16] Combining the capillary pressure curves (Figures 1 and 2) with the corresponding permittivity curves (Figures 3 and 4) results in a unique relation between P_c, S_w and ε'_s. The permittivity behavior as shown in Figures 3 and 4 looks qualitatively similar to the interfacial area data obtained from network models and micro-pore models, which show the typical smooth and non-monotonic shape [*Reeves and Celia*, 1996; *Held and Celia*, 2001; *Cheng et al.*, 2004]. For our experiments, the primary drainage and secondary imbibition curves lie on a simple plane, establishing the unique relation of capillary pressure as a function of water saturation and electric permittivity. Unfortunately, a 3-dimensional view, as presented in the work of *Reeves and Celia* [1996] and *Cheng et al.* [2004], does not graphically clarify this uniqueness. Since the low frequency ε'_s relates to polarization effects on the gas-water and water-solid interfaces, and the distribution of these interfaces contributes to the permittivity hysteresis, the electric permittivity can be seen as a measure for the interfacial area. Investigation of the exact relation between ε'_s and interfacial area is beyond the scope of this study and is therefore subject for future work.

[17] Comparing different studies on water-wet samples, it can be concluded that there is no general consensus on whether the interfacial area as function of S_w is higher for imbibition than for drainage. The same applies to the scanning curves (see Figure 4, S4c-f). The differences between our $\varepsilon'_s - S_w$ and $\alpha_{wn} - S_w$ relationships, as presented in earlier work, can be explained by the definition of the interfacial area and the assumptions that are made to define the interfacial area. *Reeves and Celia* [1996] estimated in their theoretical study the interfacial area between the water and gas phase, but they ignored the wetting films. *Cheng et al.* [2004] only described the capillary pressure dominated interface for their network model, whereas *Dalla et al.* [2002] assumed the wetting-non-wetting interface to be a function of all specific interfacial areas. Based on our findings, we propose that both the gas/liquid and the fluid/solid interfaces are necessary to provide unique relationships between capillary pressure, electric permittivity and water saturation.

5. Conclusions

[18] We have found that the low frequency ε'_s behavior can primarily be ascribed to the polarization of both the gas-water and water-solid interfaces, to different bulk phase geometries and distributions and on saturation history, which occur during drainage and imbibition. Our experimental data show that capillary pressure is a unique function of the permittivity and the water saturation. Hence, our results provide the experimental evidence that the low frequency electric permittivity is a measure to describe the interfacial area. This leads to new and important insights into the description of multiphase fluid flow in porous media and understanding of pore-scale mechanisms.

[19] **Acknowledgments.** This research was carried out as part of the CATO program (http://www.CO2-cato.nl/) and the DIOC water project. The financial support is gratefully acknowledged. We thank Leticia Moreno Tirado for her assistance and L. Vogt, P.S.A. de Vreede, H.G van Asten and H.K.J. Heller for technical support.

References

Chelidze, T. L., and Y. Gueguen (1999), Electrical spectroscopy of porous rocks: A review—I. Theoretical model, *Geophys. J. Int.*, *137*, 1–15.

Chelidze, T. L., Y. Gueguen, and C. Ruffet (1999), Electrical spectroscopy of porous rocks: A review—II. Experimental results and interpretation, *Geophys. J. Int.*, *137*, 16–34.

Cheng, J.-T., L. J. Pyrak-Nolte, D. D. Nolte, and N. J. Giordano (2004), Linking pressure and saturation through interfacial areas in porous media, *Geophys. Res. Lett.*, *31*, L08502, doi:10.1029/2003GL019282.

Dalla, E., M. Hilpert, and C. T. Miller (2002), Computation of the interfacial area for two-fluid porous medium systems, *J. Contam. Hydrol.*, *56*, 25–48.

Hassanizadeh, S. M., and W. G. Gray (1993), Thermodynamic basis of capillary pressure in porous media, *Water Resour. Res.*, *29*, 3389–3405.

Held, R. J., and M. A. Celia (2001), Pore-scale modelling extension of constitutive relationships in the range of residual saturations, *Water Resour. Res.*, *37*, 165–170.

Knight, R. (1991), Hysteresis in the electrical resistivity of partially saturated sandstones, *Geophysics*, *56*, 2139–2147.

Knight, R., and A. Abad (1995), Rock/water interaction in dielectric properties: Experiments with hydrophobic sandstones, *Geophysics*, *60*, 431–436.

Knight, R. J., and A. Nur (1987), The dielectric constant of sandstones, 60 kHz to 4 MHz, *Geophysics*, *52*, 644–654.

Morrow, N. (1970), Physics and thermodynamics of capillary action in porous media, *Ind. Eng. Chem.*, *62*, 32–56.

Plug, W. J., E. C. Slob, J. Bruining, and L. M. Moreno Tirado (2007), Simultaneous measurement of hysteresis in capillary pressure and electric permittivity for multi-phase flow through porous media, *Geophysics*, *72*(3), A41–A45, doi:10.1190/1.2714684.

Reeves, P. C., and M. A. Celia (1996), A functional relationship between capillary pressure, saturation and interfacial area as revealed by a pore-scale network model, *Water Resour. Res.*, *32*, 2345–2358.

Roberts, J. J., and W. Lin (1997), Electrical properties of partially saturated Topopah Spring Tuff: Water distribution as function of saturation, *Water Resour. Res.*, *33*, 577–587.

Ruffet, C., Y. Gueguen, and M. Darot (1991), Complex conductivity measurements and fractal nature of porosity, *Geophysics*, *56*, 758–768.

Seleznev, N., A. Boyd, T. Habashy, and S. Luthi (2004), Dielectric mixing laws for fully and partially saturated carbonate rocks, paper presented at 45th Annual Symposium, Soc. of Petrophys. and Well Log Anal., Noordwijk, Netherlands.

Ulrich, C., and L. D. Slater (2004), Induced polarization measurements on unsaturated, unconsolidated sands, *Geophysics*, *69*, 762–771.

J. Bruining, W.-J. Plug, and E. Slob, Department of Geotechnology, Delft University of Technology, Stevinweg 1, Delft NL-2628 CN, Netherlands. (w.j.plug@tudelft.nl)

J. van Turnhout, Faculty of Applied Sciences, Delft University of Technology, Julianalaan 136, Delft NL-2628 BL, Netherlands.